Available online at www.sciencedirect.com
SCIENCE DIRECT®
Applied Thermal Engineering 26 (2006) 131–143
APPLIED THERMAL ENGINEERING
www.elsevier.com/locate/apthermeng

Carbon-foam finned tubes in air–water heat exchangers

Qijun Yu [a], Anthony G. Straatman [a,*,1], Brian E. Thompson [b,1]

[a] Department of Mechanical and Materials Engineering, The University of Western Ontario, London, ON, Canada N6A 5B8
[b] Department of Mechanical Engineering, The University of Ottawa, Ottawa, ON, Canada K1N 6N5

Received 20 December 2004; accepted 1 June 2005
Available online 18 August 2005

Abstract

An engineering model is formulated to account for the effects of porosity and pore diameter on the hydrodynamic and thermal performance of a carbon-foam finned tube heat exchanger. The hydrodynamic and thermal resistances are obtained from well-established correlations that are extended herein to account for the influence of the porous carbon foam. The influence of the foam is characterized on the basis of a unit-cube geometric model that describes the internal structure, the exposed surface, the permeability and the effective conductivity as a function of porosity and pore diameter. The engineering model is validated by comparison with experiments that characterize heat transfer in an air–water radiator made from porous carbon foam. The model is also used in to conduct a parametric study to show the influence of the porosity and pore diameter of the foam. The parametric study suggests that in comparison to conventional aluminum finned-tube radiators, improvements of approximately 15% in thermal performance are possible without changing the frontal area, or the air flow rate and pressure drop. The engineering model developed herein can be used by engineers to assess quantitatively the suitability of porous carbon foam as a fin material in the design of air–water heat exchangers.

Keywords: Air–water heat exchanger; Carbon foam; Finned tube; Engineering model; Porous thermal materials

1. Introduction

Air–water heat exchangers are commonly employed in engine cooling, high-power electronics cooling, and heat recovery units for power generation systems. The resistance to convective heat transfer on the air side of the heat exchanger dominates in the design of these heat exchangers. Large numbers of impermeable metal fins are used to provide additional surface area on the air side of the heat exchanger to lower the total convective thermal resistance however the associated increase in surface area also results in large pressure drops, which must be overcome by higher fluid power input on the air side. Hence, the classical problem in heat exchanger design emerges: an optimum balance must be found between the thermal resistance (convective heat transfer) and the hydrodynamic resistance (pressure drop).

There has been recent interest in the use of porous carbon-foam fins as a replacement for aluminum fins in finned tube radiators [1]. The interest stems from the notion that the unique thermodynamic properties of the foam would serve to reduce the thermal resistance of a heat exchanger without significant additional pressure drop. As will be described in detail below, porous carbon foam has an open, interconnected internal structure and a very high specific thermal conductivity, which combined, renders the foam an interesting alternative material in heat transfer devices.

The present paper considers the use of porous carbon-foam fins in a conventional air–water heat

* Corresponding author.
E-mail addresses: qyu4@eng.uwo.ca (Q. Yu), astraatman@eng.uwo.ca (A.G. Straatman), thompson@eng.uottawa.ca (B.E. Thompson).
[1] Member ASME.

1359-4311/$ - see front matter © 2005 Elsevier Ltd. All rights reserved.
doi:10.1016/j.applthermaleng.2005.06.004

exchanger and describes the influence of the foam on the thermal and hydrodynamic resistances. Porous carbon foam is a material developed at Oak Ridge National Laboratory (ORNL). The carbon foam has an open, interconnected void structure that enables the infiltration of fluid, and a unique solid matrix derived from a carbon-foaming process, also developed at ORNL. The unique structure provides as much as 5000–50,000 [m^2/m^3] of internal surface area, which can be recruited for convective heat transfer if the fluid passes through the foam material. The effective (stagnant) conductivity of the carbon foam is in the range 40–180 [W/m K] due to the very high specific conductivity of the carbon material ($k = 900$–1700 [W/m K]) depending on the porosity which is normally between 0.7 and 0.9 using the current foaming process [2,3]. In contrast, similar porosity aluminum foams have effective conductivities of approximately 5–20 [W/m K], which result from specific conductivities of 160–230 [W/m K] for aluminum alloys. As such, the carbon foam has a much higher capability to conduct heat into its internal structure so that infiltrated fluid can convect heat away. It is because of this high effective conductivity that porous carbon foam is considered for use as a fin material. Fins of moderate height can be constructed and bonded to flattened metal liner tubes to increase the available surface area. The open structure at the air–foam interface acts as a sub-layer interrupter, which produces near-wall turbulent eddies that actively exchange energy with the porous foam surface. This, combined with the overall pressure drop across the edges of the fin leads to enhanced convective heat transfer.

This paper describes the development of engineering models that can be used to investigate air–water heat exchangers made from tubes covered with fins made from carbon foam. Although well-established correlations for air flowing over solid fins made of different materials and surface configurations are available, these do not account specifically for the effects of the pore structure on the flow and heat transfer of air flowing over fins made of carbon foam material. Thus, an objective of the research reported herein was to represent, for the purposes of engineering design, the effects of the carbon foam structure on the thermal and hydrodynamic resistances of an air–water heat exchanger. Geometric and thermophysical parameters of the carbon foam required for the heat transfer and hydrodynamic calculations are determined using the unit-cube geometric model [4], since it best represents the geometric and thermophysical characteristics of the carbon foam. A thermal–electrical analogy is employed to establish the complete heat transfer model. The separate elements of the thermal resistance are then formulated using heat transfer models that are extended to incorporate the effects of the foam porosity and void diameter. The air velocities and the hydrodynamic resistance in the porous fins and interconnected pore channels are determined by a formulation that includes the continuity equation, Darcy–Forchheimer extended equation [5] and Darcy–Weisbach equation [6]. The permeability and the Forchheimer coefficient in the Darcy–Forchheimer extended equation, and the surface roughness of the fin surface (exposed pore surface) in the Darcy–Weisbach equation are computed using the unit-cube geometric model [4].

The remaining sections of this paper describe: the details of the finned tube configuration considered, the hydrodynamic and thermal resistance models; validation of the complete model by comparison to test cases of a carbon-foam finned air–water heat exchanger [1]; the results of a parametric study and conclusions. The parametric study was conducted to show how the foam porosity and void diameter and the fin height, width and spacing influence the performance of a carbon-foam finned air–water heat exchanger. The parametric study isolates the different influences of the carbon foam and quantifies the benefits that can be realized so that decisions can be made as to the suitability of carbon foam in a conventional radiator design.

2. Finned tube configuration

A simple straight fin with a uniform cross-section attached to a flattened liner tube is the finned-tube configuration chosen for the present study based on the mechanical properties of the carbon foam, the flow and heat transfer behaviour, and the bond contact quality and manufacturing cost including materials and labour. Fig. 1(a) shows the details of the finned tube configuration. The fins have a rectangular shape with straight uniform cross-sections, and are attached to the outside surface of the liner tubes. Fig. 1(b) shows detailed dimensions of the finned tube configuration: H_F is the carbon foam fin height; T_F the fin thickness; L_F the fin length along the air flow direction; F_{BH} the height of the carbon foam base plate; F_{SP} the space between two adjacent fins; F_{TP} the tip clearance between the fins of two finned tubes; T_W the wall thickness of the flattened liner tube; and D_I the inside diameter of the flattened liner tube.

3. Hydrodynamic model

A hydrodynamic model is required to calculate the air pressure drop for a given geometry and flow condition. In the present case, the geometry is dependent upon the fin size and spacing, and the porosity and void diameter of the porous carbon foam used to construct the fins, since the structure of the foam affects the fluid infiltration and the interface between the foam and the airflow. Fig. 2 gives an approximation of the air velocity

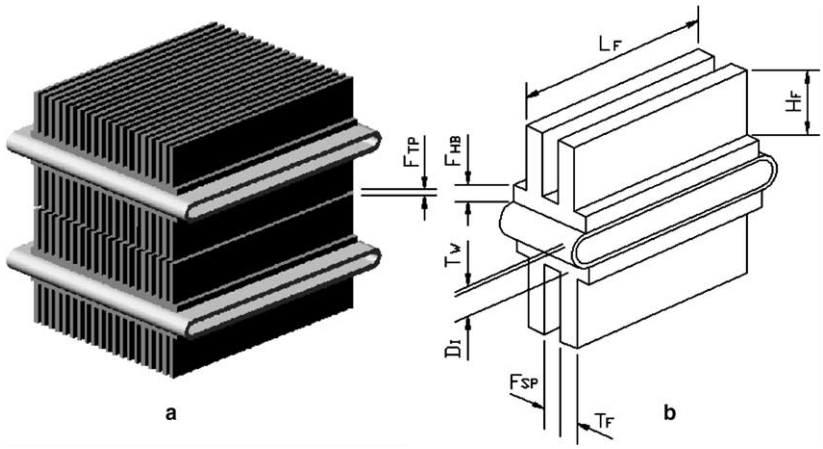

Fig. 1. (a) Rectangular finned, flattened tube configuration; (b) detailed dimensions of the finned configuration.

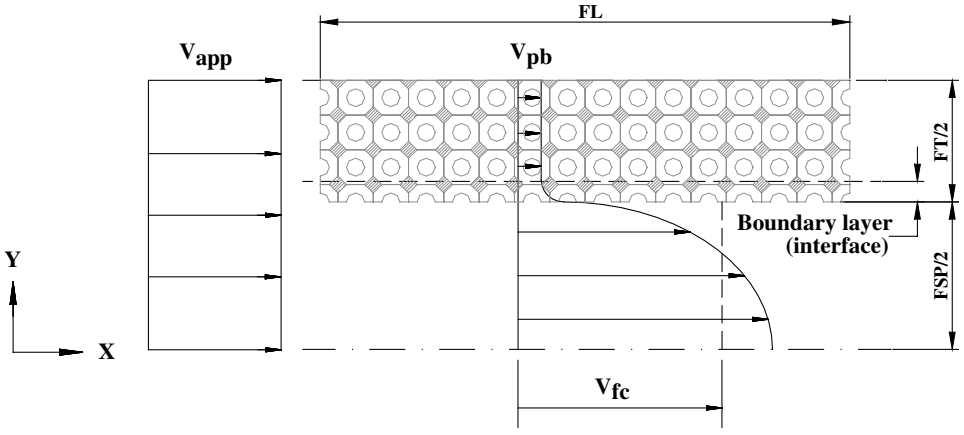

Fig. 2. Approximation of air velocity profile in the fin and inter-connected pore channels.

profile for air flowing through the fins made from porous materials [7]. Here, V_{pb} is the air velocity in the inter-connected pore channel, also called the air filter velocity, and V_{fc} is the air mean velocity in the fin channel. V_{pb} and V_{fc} can be determined by solving the continuity, Darcy–Weisbach [6] and Darcy–Forchheimer [5] equations:

$$\nabla(\rho V) = 0 \tag{1}$$

$$\Delta P = \left(f\frac{L_F}{D_{fch}} + \sum C\right)\frac{\rho}{2}V_{fc}^2 \tag{2}$$

$$\frac{\Delta P}{L_F} = \frac{\mu}{K}V_{pb} + \frac{c_f}{\sqrt{K}}\rho V_{pb}^2 \tag{3}$$

where ρ and μ are the fluid density and viscosity, respectively, V is the mass velocity and ΔP is the pressure drop across the fin bank. For $Re_L < 1500$, the friction factor is obtained from $f = 64/Re_L$. For higher Re_L, the friction factor f of the fin channel in Eq. (2) can be determined by Altshul's equation [6]:

$$f = 0.11\left(\frac{R_A}{D_{fch}} + \frac{68}{Re_L}\right)^{0.25} \tag{4}$$

where D_{fch} is the equivalent hydraulic diameter of the fin channel, $Re_L = V_{fc}L_c/v$ is the Reynolds number in the fin channels, L_c is the characteristic length and v is the kinematic viscosity of air evaluated at the average air temperature. In the implementation of the friction factor, for Re_L near 1500, the results of the laminar and turbulent expressions are blended so that step changes in the pressure drop do not occur. K, c_f and R_A are the permeability, the Forchheimer coefficient and the fin surface roughness due to the exposed pores, respectively, all of which are determined using expressions derived from the unit-cube geometry model [4]:

$$K = \frac{36\varepsilon^3}{147\beta^2} \tag{5}$$

$$c_f = 0.0928\frac{1}{\varepsilon^{3/2}} \tag{6}$$

$$R_A = \frac{1}{2}\sqrt{D^2 - H^2} \tag{7}$$

In Eqs. (5)–(7), ε is the porosity, β is the internal area factor, D is the void diameter of the foam and H is the dimension of the unit cube. The area factor β is

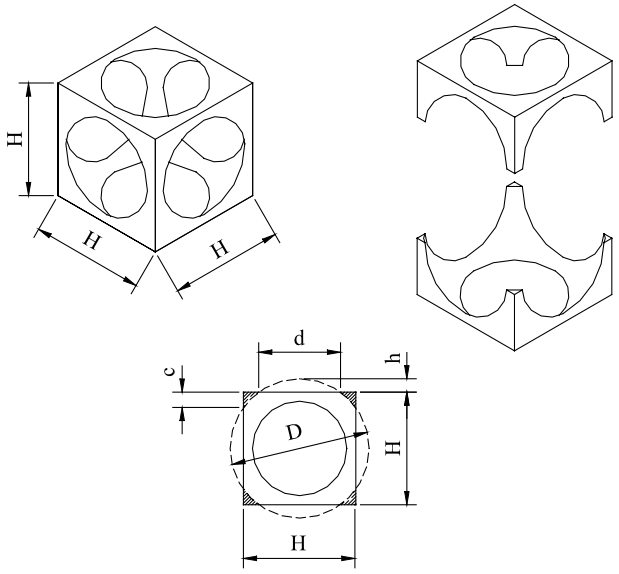

Fig. 3. Detailed dimensions of the Unit Cube Geometry Model [4] for a cross-sectional cut at the centre plane of the unit cube.

the interior surface area to volume ratio of the foam and is determined by [4]:

$$\beta = \frac{\pi D}{H^3}(3H - 4D) \tag{8}$$

The dimension H is illustrated in Fig. 3 and is determined by solving a cubic equation obtained from the definition of the porosity of porous media [4]. The effects of the carbon foam structure on the hydrodynamic resistance in the fin channel are taken into account inherently by the variables incorporated in Eqs. (2) and (3). Modification of the porosity and void diameter directly affect all the geometric parameters of the foam and the air velocities, and therefore the hydrodynamic resistance across the heat exchanger.

The pressure drop across the fin channels and the fins themselves (in the flow direction) is always the same and is equal to the overall pressure drop of the system. Thus, Eqs. (1)–(3) represent a closed system of equations for ΔP, V_{pb} and V_{fc}. The solution is obtained by equating Eqs. (2) and (3) and expressing one velocity in terms of the other using Eq. (1). The remaining variables can then be calculated explicitly.

4. Thermal model

Convective and conductive heat transfer are both important in the exchange of heat in finned, flattened tube heat exchangers. Convection transfers heat from the surface of the tube walls and the surface of the fins, to fluid passing through the fin channel and, in the present case, through the inter-connected pores. Conduction transfers this heat through the liner tube walls, the bond contact layers, the fin base plate and the fin body, and the fouling layers on the tube and the fin sides.

The governing equation used in the design of heat exchangers is expressed in the general form: $q = UA\Delta T_m$, where U is the overall heat transfer coefficient based on the fin side total heat transfer surface area A, and ΔT_m is the mean temperature difference between the two fluids on the tube and fin sides. The governing equation can also be written as

$$q = \frac{\Delta T_m}{R_t} \tag{9}$$

where R_t is the total thermal resistance, which can be obtained from a thermal–electrical analogy of the heat exchanger. The thermal circuit for the present case is shown in Fig. 4. The resistances are described in detail in Fig. 4. The resistances R_9, R_{10}, R_{11}, R_{12}, R_{15} and R_{16}, are practically negligible compared to the dominant resistances in the thermal circuit. Thus, to simplify the overall thermal circuit, these minor resistances are lumped into the overall system by adding their surface areas to R_7, R_8, R_{17} and R_{18}, which is reasonable since all of these minor resistances are connected in parallel with the main heat path. The simplified thermal circuit is presented in Fig. 5. The total thermal resistance of the circuit is then expressed as

$$R_t = R_{123} + \left(\frac{1}{R_{910}} + \left(R_{456} + \left(\frac{1}{R_{78}} + \frac{1}{R_{1112}}\right)^{-1}\right)^{-1}\right)^{-1} \tag{10}$$

where $R_{123} = R_1 + R_2 + R_3$ is the total thermal resistance at the water side in the main heat path including the convection resistance at the tube side R_1, fouling resistance at the tube side R_2 and the conduction resistance through the liner tube wall R_3, all connected together in series; $R_{456} = R_4 + R_5 + R_6$ is the total thermal resistance in the main heat path consisting of the bond contact R_4 and fin base conduction R_5 as well as the fin base constriction R_6 due to the cross-sectional area changes at the fin root that are again connected together in series; $R_{78} = R_7 + R_8$ is the total thermal resistance of the fin channel in the main heat path including the convection R_8 and fouling R_7 resistances in the fin channel that are in series with one another; $R_{910} = R_9 + R_{10}$ is the total thermal resistance of the major resistance for the bare tube including convection R_{10} and fouling R_9 resistances connected to each other in series; and $R_{1112} = R_{11} + R_{12}$ is the total thermal resistance for the inter-connected pore channel including the convection R_{12} and fouling R_{11} resistances that are connected to each other in series. Note that R_{910} is connected with the main heat path in parallel at the location between R_{123} and R_{456}, and R_{1112} is connected with the main heat path in parallel at the location between R_{456} and R_{78}.

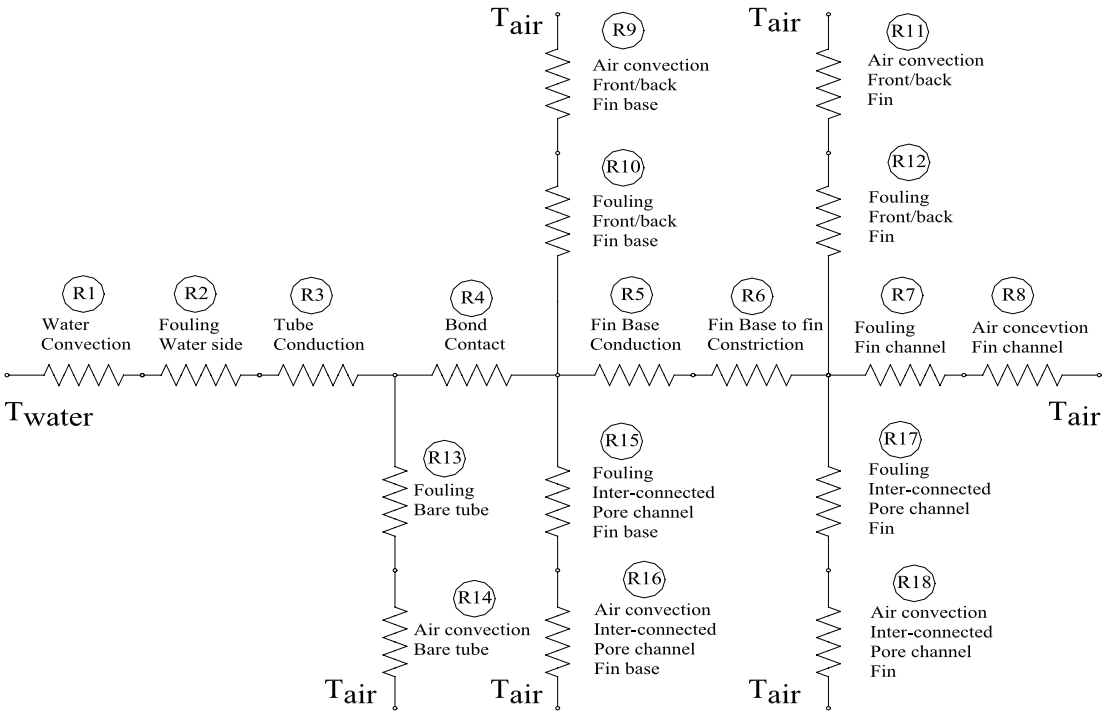

Fig. 4. Thermal resistance circuit for the rectangular finned flattened tube configuration.

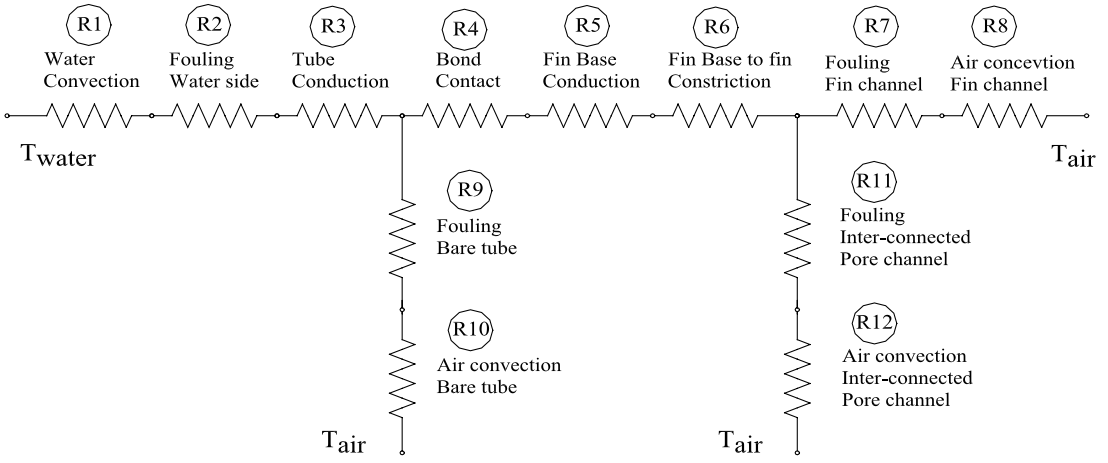

Fig. 5. Simplified thermal resistance circuit for the rectangular finned flattened tube configuration.

While the thermal circuit has been reduced to 5 main resistance elements, there are 12 individual thermal resistances in Fig. 5 that need to be formulated in terms of the geometry, the flow conditions and, where necessary, the parameters of the porous carbon foam. The resistances R_5, R_6, R_8 and R_{12} are all affected by the parameters of the carbon foam. The focus of this section is to describe in detail the modifications to these resistance models that are required to incorporate the effects of the porous carbon foam. The resistances that are not influenced by the carbon foam are described first, and are followed by a more detailed description of the other resistances listed above.

The water side convection resistance, R_1, is expressed as $R_1 = D_h/A_{ti}k_w\overline{Nu}_w$, where D_h is the hydraulic diameter of the liner tube, A_{ti} is the total inside surface area of the liner tube, k_w is the thermal conductivity of the water, and $\overline{Nu}_w$ is obtained from the Sieder–Tate equation [8] for laminar flow ($Re < 3000$) and from the Gneilinski equation [9] for turbulent flow ($Re \geqslant 3000$). The fouling resistance, R_2 is modelled using $R_2 = r_{wf}/A_{ti}$, where r_{wf} is the fouling factor [10]. The fouling resistances R_7, R_9 and R_{11} are modelled using the same expression, but accounting for the difference fouling factors and exposed surface areas. The tube conduction resistance R_3 is expressed as $R_3 = T_W/kA_{ti}$, where k is the conductivity

of the wall material. The bond contact resistance is obtained from $R_4 = T_b/k_b A_{tb}$, where T_b is the bond thickness, k_b is the thermal conductivity of the bond material and A_{tb} is the area of the bond surface. The convective resistance of the bare tube, R_{10} is modelled using $R_{10} = D_{bo}/A_{bo}k_a\overline{Nu}_a$, where D_{bo} is the diameter of the front edge of the liner tube, A_{bo} is the area of the front and back edges of the liner tube, k_a is the thermal conductivity of air and the average Nusselt number is obtained from Churchill and Bernstein [11].

4.1. Fin base conductive resistance, R_5

The fin base conduction is modelled using the conventional expression:

$$R_5 = \frac{H_{BH}}{k_e A_{tb}} \tag{11}$$

where k_e is the effective conductivity of the carbon foam obtained from [4]:

$$k_e = (1 - 2t - 2t^2)\left(\frac{\left(\frac{1}{t} - 1\right)^2 + \sigma}{\left(\frac{1}{t} - 1\right)^2 + 1}\right)k_f + \frac{2t(1-t)}{(1-t)\sigma + t}k_s \tag{12}$$

Here, k_f and k_s are the thermal conductivities of the fluid (void) and the solid, σ is the ratio k_f/k_s, $t = 2a/H$ is the normalized thickness of the ligament of the foam solid, a is the equivalent thickness of the ligament of the foam and H is the dimension of the unit cube, all obtained from expressions derived in [4]. Changes to the porosity, void diameter and the solid phase thermal conductivity directly affect the effective conductivity and, therefore the resistance due to the fin base conduction.

4.2. Fin base constriction resistance, R_6

The thermal resistance due to the change in cross-sectional area at the fin base is modelled using the expression derived by Yovanovich [12]:

$$R_6 = \frac{\left(\left(\zeta + \frac{1}{\zeta}\right)LN\left(\frac{1+\zeta}{1-\zeta}\right) + 2LN\left(\frac{1-\zeta^2}{4\zeta}\right)\right)}{2\pi k_e A_{tb} F_{PM}} \tag{13}$$

where F_{PM} is the fin density (number of fins per meter of the length of the liner tube) and ζ is the relative contact size and is defined by

$$\zeta = \frac{T_F}{T_F + F_{SP}} \tag{14}$$

Again, modifications to the porosity and void diameter affect the effective conductivity, k_e, which produces an influence in R_6.

4.3. Convective resistance in the fin channel: R_8

The convective resistance in the fin channel is affected by both the roughness of the exposed surface and by the effective surface area of the air–foam interface. The thermal resistance due to convection, R_8, is expressed as

$$R_8 = \frac{L_c}{\eta_o A_{to} k_a \overline{Nu}_a} \tag{15}$$

where L_c is a characteristic length scale that depends on the Reynolds number, η_o is the overall surface efficiency, A_{to} is the total heat transfer surface area, k_a is the thermal conductivity of air evaluated at the average air temperature, and $\overline{Nu}_a$ is the average Nusselt number, which is also dependent upon the Reynolds number. The overall surface efficiency η_o is given by

$$\eta_o = 1 - \frac{A_{tb}}{A_{to}}(1 - \eta_f) \tag{16}$$

where A_{tb} is the total primary surface area at the air side and η_f is the fin efficiency. The total heat transfer surface area at the exposed pore surface of the fin, A_{to}, is determined by

$$A_{to} = S_F A_{tf} \tag{17}$$

where S_F is the surface area factor of the exposed pore surface, which is a function of the porosity and void diameter of the foam, and A_{tf} is the total plan area of the fin. Fig. 6 shows the relationship between the surface area factor and the porosity [4] (the influence of pore diameter is less significant and not shown). The fin efficiency η_f is determined by

$$\eta_f = \frac{\tanh\sqrt{2Nu_i \frac{k_a}{k_e}\frac{H_{Fe}}{L_c}\frac{H_{Fe}}{T_F}\left(1 + \frac{T_F}{L_{Fe}}\right)}}{\sqrt{2Nu_i \frac{k_a}{k_e}\frac{H_{Fe}}{L_c}\frac{H_{Fe}}{T_F}\left(1 + \frac{T_F}{L_{Fe}}\right)}} \tag{18}$$

where Nu_i is the ideal Nusselt number (described below) and H_{Fe} and L_{Fe} are the effective fin height and fin length, respectively. Since the fin efficiency is a function of the effective conductivity, k_e, and the Nusselt number, the influence of the porous carbon foam is implicitly accounted for in this expression.

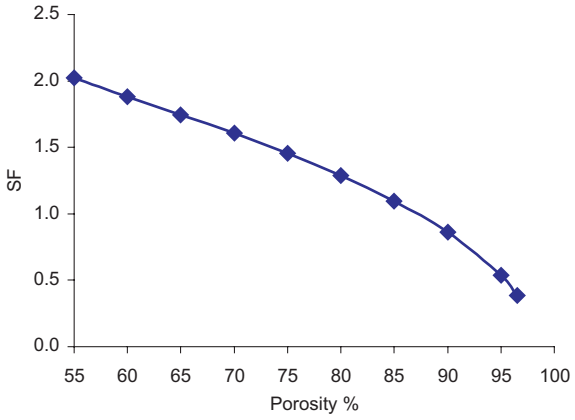

Fig. 6. Surface area factor at exposed pore surface as a function of porosity [4].

The Reynolds number in the fin channel is calculated in terms of the velocity, V_{fc}, which is obtained from the hydrodynamic resistance model described in Section 3 above, and the hydraulic diameter of the fin channel. For $Re_L \leqslant 1500$, the flow is assumed laminar despite the surface roughness, i.e., the flow is assumed to be parallel to the walls and the influence of the surface roughness does not in itself modify the near-wall flow. The effect of the porous carbon foam is accounted for by the modified surface area described in Eq. (17). Thus, for the laminar regime, the characteristic length is $L_c = F_{SP}$ and the average Nusselt number in the fin channel is determined by the process proposed by Teertstra [13]:

$$\overline{Nu}_a = \eta_f Nu_i \tag{19}$$

where the ideal Nusselt number, Nu_i, is obtained from [13]:

$$Nu_i = \left[\left(\frac{Re_b^* Pr}{2}\right)^{-3} + \left(0.664\sqrt{Re_b^*}Pr^{1/3} \times \sqrt{1+\frac{3.65}{\sqrt{Re_b^*}}}\right)^{-3}\right]^{-1/3} \tag{20}$$

Here, Re_b^* is the modified Reynolds number determined by $Re_b^* = Re_b F_{SP}/L_F$, where the characteristic length used in the Reynolds number Re_b is the fin spacing F_{SP}, i.e., the distance between two fins.

For $1500 < Re_L < 3000$, the flow is considered transitional. When the flow is transitional, the near-wall flow is interrupted by the rough foam surface and assumed to become turbulent like. The condition of the main (finned-channel) flow is not yet assumed to a function of the surface condition. Thus, beyond the area factor (Eq. 17), the additional influence of the carbon foam for transitional flow is accounted for using a convection correlation for turbulent flow. In this case, the characteristic length is $L_c = D_{fch}$ and the average Nusselt number is obtained from the Dittus–Boelter equation [14]:

$$\overline{Nu}_a = 0.0243 Re^{0.8} Pr^n \tag{21}$$

where $n = 0.4$ for air cooling applications for which the water inlet temperature is greater than the air inlet temperature and $n = 0.3$ for air heating applications for which the water inlet temperature is lower than air inlet temperature.

For $Re_L \geqslant 3000$, the flow is considered fully turbulent. For fully turbulent flow, the near-wall eddies actively utilize the full exposed surface area and the flow itself is affected by the surface condition, which is controlled by the surface roughness. To account for this, the characteristic length scale is computed from $L_c = D_{fch}$, as for transitional flow, and the Nusselt number is obtained from the Gnielinski equation [9]:

$$\overline{Nu}_a = \frac{(f/8)(Re_L - 1000)Pr}{1 + 12.7\sqrt{f/8}(Pr^{2/3} - 1)} \tag{22}$$

The dependence of the friction factor on the foam porosity and void diameter is described in Section 3 above. As in the laminar and transitional regimes, the modified surface area given in Eq. (17) is used as the total exposed surface for heat transfer. Thus, for fully turbulent flow the influence of the carbon foam is accounted for by a modified surface area and by the friction factor in Eq. (22), both of which depend upon the parameters of the carbon foam.

In the implementation of the convective heat transfer relations, care was taken to ensure that smooth transitions occurred near the limits of the correlations used, i.e., the transition from laminar to transitional flow ($Re = 1500$) and transitional to fully turbulent flow ($Re = 3000$). Near these points, solutions from above and below the transition points were blended to give a reasonable estimate of the Nusselt number.

4.4. Convective resistance in the interconnected pore channel: R_{12}

There is an additional heat transfer that takes place in the interconnected pore channel due to the interstitial flow through the carbon matrix caused by the pressure gradient across the fin bank. The additional heat transfer is taken into account in the present engineering model by adding the convective resistance of the interconnected pore channel R_{12} as a branch parallel to the convective resistance of the fin channel R_8 as shown in Figs. 4 and 5. The convective resistance of the interstitial flow in the interconnected pore channel is approximated by

$$R_{12} = \frac{D_E}{\eta_o A_{tpb} k_{af} \overline{Nu}_{sf}} \tag{23}$$

where the overall surface efficiency η_o is determined by Eq. (16) based on the assumption that the temperature distribution of the carbon foam fin body is controlled by the convection in the fin channel. A_{tpb} is the total interior heat transfer surface available in the interconnected pore channel and is determined by

$$A_{tpb} = \Lambda_t \beta \tag{24}$$

where Λ_t is the total volume of the foam available for the interstitial flow through the fin body and β is the interior surface area to volume ratio of the foam determined by Eq. (8) [4]. k_{af} is the thermal conductivity of air evaluated at the film temperature and $\overline{Nu}_{sf}$ is the pore-level average Nusselt number, which is dependent upon the pore-level Reynolds number, $Re_d = V_{pb} D_E/\nu$. Here D_E is the equivalent particle diameter obtained from [15]:

$$D_E = \frac{6(1-\varepsilon)}{\beta} \tag{25}$$

For $Re_d \leqslant 75$, the average pore-level Nusselt number is obtained from [16,17]:

$$\overline{Nu}_{sf} = 0.004\left(\frac{d_v}{D_E}\right)^{0.35} Re_d^{1.35} Pr^{1/3} \tag{26}$$

where d_v is the equivalent diameter of the void phase determined by [4]:

$$d_v = \sqrt[3]{\frac{6\varepsilon}{\pi}} H \tag{27}$$

For $Re_d \geqslant 350$ the average pore-level Nusselt number is obtained from [18]:

$$\overline{Nu}_{sf} = 1.064 Re_d^{0.59} Pr^{1/3} \tag{28}$$

For $75 < Re_d < 350$, linear interpolation between Eqs. (26) and (28) is to be used [19]. As such, the influence of the porosity and void diameter is accounted for in the thermal resistance due to interstitial flow in the interconnected pore channel (fin body).

5. Validation of the engineering models

The proposed hydrodynamic and thermal models are validated by comparison with measurements from an air–water radiator constructed using carbon-foam finned tubes [1]. Fig. 7 shows the air radiator and the test set-up. This radiator consists of four cores in parallel at the tube side. Each core has an overall width of 305 mm, a height of 76 mm and consists of seven aluminum liner tubes with carbon-foam fins brazed to them. Table 1 summarizes the detailed geometry specification of the carbon-foam finned air–water radiator tested by [1]. The tube side fluid is a glycol–water mixture with a volume ratio of 20/80. An axial fan with a DC motor (VA18-AP6-41MA built by SPAL) is used to supply air to the fin side of the air–water radiator. Fig. 8 gives the fan performance curve in terms of volume flow rate and static pressure. Table 2 gives a summary of the operating conditions and measured results for two experiments, and the predictions from the present engineering models. In terms of the air-side Reynolds numbers, the model predictions are based on the transitional formulation

Table 1
Summary of specifications of the air–water heat exchanger built and tested by Ott et al. [1]

Items	Specification
1. Carbon foam pore structure	
1.1 Pore diameter (μm)	350.00
1.2 Porosity (%)	75.00
1.3 Solid graphite thermal conductivity at room temperature (W/m K)	1200.00
2. Fin configurations	
2.1 Fin thickness (mm)	1.016
2.2 Fin density (fin number per meter length of liner tube covered by fins) (F_{PM})	295.28
2.3 Fin height (mm)	3.175
2.4 Fin length (along air flow direction) (mm)	304.80
2.5 Fin base plate (carbon foam) height (mm)	0.7938
2.6 Fin tip clearance (mm)	0.7938
3. Liner tube configuration	
3.1 Liner tube inside diameter (mm)	2.3813
3.2 Liner tube wall thickness (mm)	0.7938
3.3 Thermal conductivity of liner tube (AL-6101) (W/m K)	180.00
4. Core size	
4.1 Core front face length (tube length) (mm)	304.80
4.2 Core front face width (mm)	76
4.3 Tube number at core face	7
5. Heat exchanger	
5.1 Core number	4
5.2 Flow arrangement	Crossflow
5.3 Passes of water side (tube side)	4
5.4 Total liner tube number	28

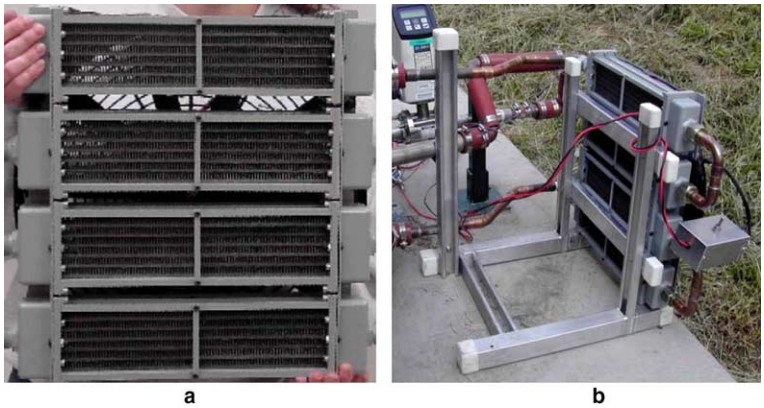

Fig. 7. (a) A prototype of an air radiator made from carbon-foam finned tubes [1]; (b) test set-up for thermal performance measurements.

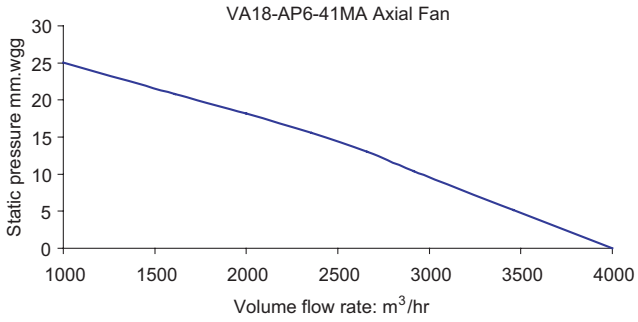

Fig. 8. Fan performance curve for the VA18-AP6-41MA axial fan used in [1].

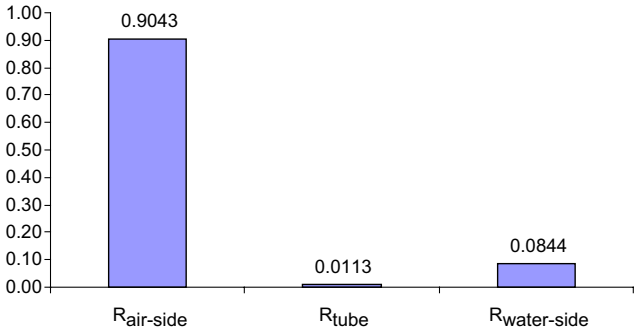

Fig. 9. Distribution of major thermal resistances predicted using the present thermal engineering model for the carbon-foam finned radiator [1] for thermal conditions corresponding to Test 3 (foam).

of the hydrodynamic and thermal resistances. Table 2 indicates that the air pressure loss predicted by the present model is about 13.5% higher than that obtained from the fan curve under operating conditions of Test 3 (foam). Since there is no fan data available for Test 2 (foam), validation of the pressure-drop is not possible. In terms of the thermal performance, Table 2 indicates that for Test 3 (foam), the present thermal engineering model predicts a heat load that is 5.9% lower than that measured and for Test 2 (foam), a heat load that is 8.6% lower than the measured result. Thus, the present hydrodynamic and thermal models give predictions that are conservative and, notably, within the conventional thermal engineering standard of 20%.

It is also of interest to illustrate what elements of the thermal circuit dominate the thermal resistance of the carbon-foam finned air–water radiator. From the outset, porous carbon foam was used in an attempt to reduce the air-side thermal resistance thereby improving the overall performance of the radiator. Fig. 9 shows the dominant resistances in the thermal circuit for the air–water heat exchanger as predicted from the present thermal engineering model for thermal conditions of Test 3 (foam). The figure shows that the air-side thermal resistance still comprises more than 90% of the total thermal resistance while the water side comprises only about 8%, and the remaining resistances sum to less than 2% of the total thermal resistance. This implies one of two things: that the carbon-foam fins do not serve to reduce the thermal resistance of the radiator or that the radiator has not been designed using the optimal set of geometric parameters. The next section considers both of these possibilities. A parametric study is conducted using the proposed hydrodynamic and thermal engineering models to investigate the influence of the foam porosity and pore diameter and the fin height, thickness and spacing on the performance of a carbon-foam finned tube heat exchanger operating under the same conditions given in Table 2.

6. Parametric study and alternate design for carbon foam core

The main focus of the present parametric study is to use the proposed hydrodynamic and thermal engineering models to illustrate the influence of the carbon foam and geometric parameters on the performance of a carbon-foam finned air–water radiator. Since there are five separate parameters considered, the parametric study is done using the orthogonal method [20]. Due to the range of parameters considered, the air-side Reynolds number is in the range 400–2600 and thus model predictions are obtained from both the laminar and transitional formulations.

Table 2
Summary of test conditions and thermal performance data from Ott et al. [1] (measured), and predictions from present engineering models

Items	Test 3 (foam)			Test 2 (foam)		
	Measured	Present model	Error	Measured	Present model	Error
Water in temp. (°C)	98.8	98.8	–	80.1	80.1	–
Water out temp. (°C)	86	86.7492	0.87 %	67.7	68.7727	1.58 %
Water flow (kg/s)	0.29	0.29	–	0.12	0.12	–
Water pressure loss (kPa)	N/A	1.44		N/A	0.27	
Air in temp. (°C)	31.6	31.6	–	32.2	32.2	–
Air flow (kg/s)	0.69	0.69	–	0.36	0.36	–
Air pressure loss (mm H_2O)	17.2[a]	19.52	1.1349	N/A	5.69	
Heat load (kW)	14.82	13.9529	0.9415	5.931	5.4185	0.9136

[a] Obtained from the fan curve, as shown in Fig. 8, provided by the fan manufacturer SAPL.

Table 3
Orthogonal design table for five factors with four levels—OA16542 or $L_{16}(4)^5$-2

Treatments	Factors				
	A	B	C	D	E
	Pore dia. (μm)	Porosity (%)	Fin Tk. (mm)	Fin Ht. (mm)	FPM
1	250	79	0.953	6.350	464
2	250	69	0.727	7.269	354
3	250	60	0.832	8.321	532
4	250	90	0.635	9.525	406
5	375	79	0.727	8.321	406
6	375	69	0.953	9.525	532
7	375	60	0.635	6.350	354
8	375	90	0.832	7.269	464
9	328	79	0.832	9.525	354
10	328	69	0.635	8.321	464
11	328	60	0.953	7.269	406
12	328	90	0.727	6.350	532
13	286	79	0.635	7.269	532
14	286	69	0.832	6.350	406
15	286	60	0.727	9.525	464
16	286	90	0.953	8.321	354

The $L_{16}(4)^5$-2 or OA(16542) table [20] is chosen for the parametric study presented here. Table 3 shows the orthogonal design table for five factors (parameters) with four levels. Each factor has the same range (1.5) with the same level segment ratio of $1.5^{1/3}$. The parametric study is carried out using the same core front dimensions as the air–water radiator described in [1] at the thermal conditions of Test 3 (foam).

Fig. 10 shows the influence of the five factors considered on the heat load of the air–water radiator in terms of an influence rating and a plot showing the variation of heat load over the range of the parameter considered. The influence rating characterizes the importance of a parameter with respect to other parameters in terms of the rate at which the outcome varies over the range of the parameter considered. Based on the influence ratings and the plots shown in Fig. 10a–c, the porosity is the main controlling factor that influences heat load, followed by the fin density and the fin thickness. The fin height and the pore diameter do not have much influence on the heat load, as can be observed by the small influence ratings and the flatness of the curves in Fig. 10d and e. It is not surprising that the porosity of porous fins has such a strong influence on the heat load. The porosity affects the thermal resistance through its influence on the internal and exposed surface area available for heat transfer, both of which decrease with increasing porosity, and through its effect on the effective conductivity on the fin, which modifies the fin efficiency. Fig. 10 suggests that for the fin configuration considered, a lower porosity is best, however this makes it more difficult for air to pass through the porous fins; most of the air passes through the fin channels and is exposed to the external surface of the fin. The positive influence of the fin thickness on the thermal performance is not surprising on the basis that thicker fins occupy more volume and, therefore, have more internal surface area (up to 5000–50,000 m^2/m^3). When the fins are thicker, a higher proportion of the airflow passes through them and the area exposure is higher. In addition, for a given fin height, a higher fin thickness yields a higher fin efficiency, which also has a positive influence on thermal performance. Note that the lowest thermal resistance would be obtained using a single fin for each tube since in this case all of the airflow would be forced through the foam where the surface area available for heat transfer is extremely high. Increasing fin density also has a positive effect on the thermal performance, but in this case in the more conventional sense that more fins gives more surface area. Improvements in the ther-

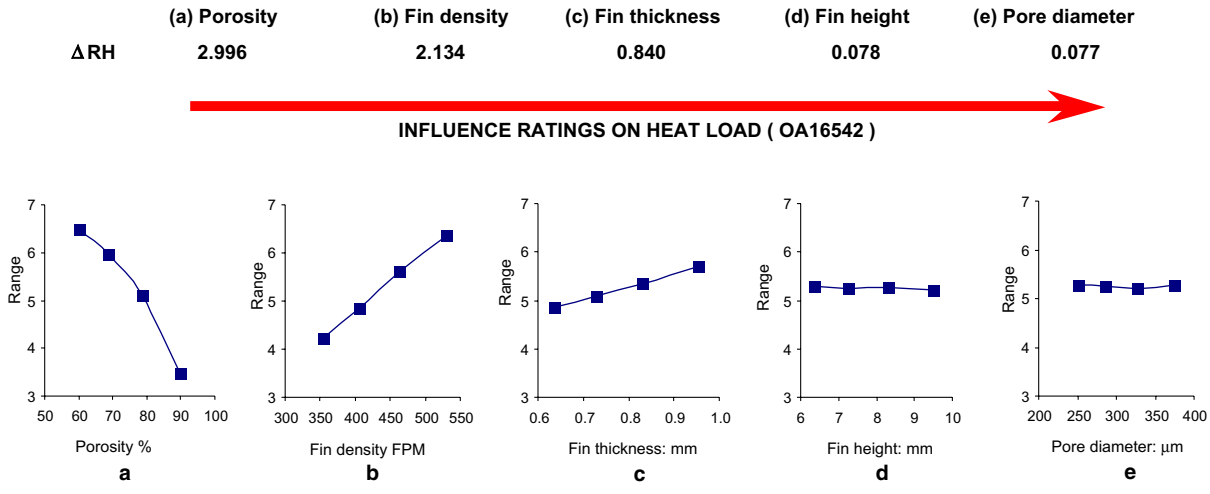

Fig. 10. Influence ratings and plots illustrating the effects of (a) porosity, (b) fin density, (c) fin thickness, (d) fin height, and (e) pore diameter on the heat load.

mal performance of the radiator have an influence on the hydrodynamic performance. Intuitively, the best condition for thermal performance, i.e. forcing all of the airflow through a single thick fin, will lead to the worst possible condition for the hydrodynamic performance.

Fig. 11 shows the importance of the five factors that influence the air pressure loss, and the effect of each factor on the air pressure loss. In this case, the fin density is the first controlling factor, followed by the fin thickness and the pore diameter. The fin height and the porosity have a much smaller influence on the air pressure loss. In terms of airflow, using more fins or thicker fins yields less open area for air to pass through, thereby producing a higher pressure drop across the radiator. With this higher pressure drop, a higher proportion of air passes through the carbon-foam fins. The influences of porosity and pore diameter on the air pressure drop are reversed with respect to their influence on thermal performance. In terms of pressure drop, increases in the pore diameter increase the surface friction factor (see Eq. (4)), which translates into higher pressure losses. Increases in porosity have a small effect on the surface friction factor, but have a large effect on the openness of the porous fins. Because the proportion of air passing through the fins is small compared to that passing through the fin channels, the influence of porosity on the overall air pressure drop is lower than that of pore diameter. If the single-solid fin case described above were considered, the porosity would have a much higher influence than the pore diameter, since the surface of the foam would no longer be a factor.

The orthogonal design process serves to establish the best combination of parameters for the configuration considered, and for our case, the biggest impact that can be expected if porous carbon foam were used as a fin material. To characterize this impact, a carbon-foam finned air–water radiator is developed to replace the standard aluminum fin air–water radiator tested in [1] for the conditions described in Test 1 (std). While the frontal area, depth and air pressure drop of the original aluminum core are maintained, the optimized pore structure and fin parameters for the air–water radiator are obtained from analysis of the outcomes of the orthogonal design processes illustrated in Figs. 10 and 11. The carbon-foam finned radiator is developed in manner similar to that described in [1] and as such, consists of four parallel cores of width 530 mm, height 119 mm and depth 50.8 mm. First, a fin porosity of 70% is selected on the basis that Fig. 10 shows that lower porosity leads to a higher heat load, and from the practical consideration that 70% is the lowest porosity that has been produced to date with current material fabrication processes for carbon foam. Because of the porous nature of the foam and the strength of the carbon matrix, the fin thickness must be greater than 2.5 times the pore diameter. From Fig. 11, it is shown that when the pore diameter is approximately 300 μm, the air pressure loss is at its lowest value. Thus a pore diameter of 300 μm is selected yielding a fin thickness of 0.762 mm. The fin height does not affect either the heat transfer or the air pressure loss as much as other factors, however, the lowest air pressure losses occur between fin heights of 8–10 mm (see Fig. 11). Therefore, a fin height of 8.725 mm is selected, which requires five tubes at the front face of each core. The fin density is set to 748 fins/m to maintain the air pressure loss of 14.2 mm wg obtained from the fan curve at the thermal conditions of Test 1 (std). Table 4 gives a summary of the thermal conditions of Test 1 (std), the thermal performance measured for the standard aluminum fin radiator, and the performance predictions for the carbon-foam finned

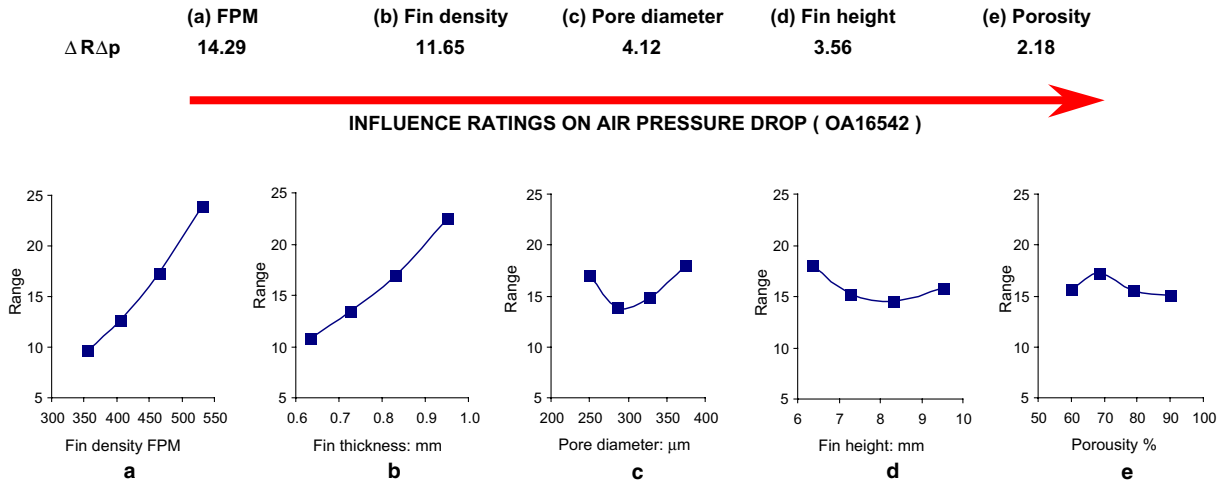

Fig. 11. Influence ratings and plots illustrating the effects of (a) fin density, (b) fin thickness, (c) pore diameter, (d) fin height, and (e) porosity on the air pressure loss.

Table 4
Comparison of the thermal performance of the standard aluminum fin radiator considered in [1] with the optimized carbon-foam finned heat exchanger for the conditions of Test 1 (std)

Items	Standard aluminum fin	Carbon foam fin	Improvement
Water in temp. (°C)	79.9	79.9	–
Water out temp. (°C)	63.1	60.6189	−2.4811 °C
Water flow (kg/s)	0.26	0.26	–
Water pressure loss (kPa)	N/A	2.1	
Air in temp. (°C)	39.5	39.5	–
Air flow (kg/s)	0.74	0.74	–
Air pressure loss (mm H_2O)	14.2[a]	14.15	–
Heat load (kW)	16.555	19.0275	1.1494

[a] Obtained from the fan curve, as shown in Fig. 8, provided by the fan manufacturer SAPL.

air–water radiator. The optimized carbon-foam finned radiator is shown to dissipate about 15% more heat than the standard aluminum finned radiator under the same air flow rate and pressure drop. Fig. 12 shows the distribution of the dominant resistances for the alternate carbon foam fin design. In comparison to Fig. 9, the air-side resistance has dropped significantly in the overall balance, which suggests that a better balance has been struck between the water and air-side thermal resistances to achieve the improvements in overall thermal performance.

It is clear from the present analysis that the use of foam fins leads to some improvement in the overall performance of an air–water radiator. Thus, if the additional effort to produce the radiator can be justified, or if weight is a primary constraint, it is possible to benefit from the use of porous carbon-foam fins. The present analysis also makes it clear, however, that the improvement from the carbon foam is mainly due to the increased surface area made available and in the present application only a small proportion of the total available surface area of the carbon foam is utilized; most of the air passes through the fin channels and not through the foam fins. Because of the unique combination of high thermal conductivity and open, interconnected structure, it is likely that entirely different designs could be conceived that take better advantage of the internal structure of the foam and rely less on the passage of air across the foam.

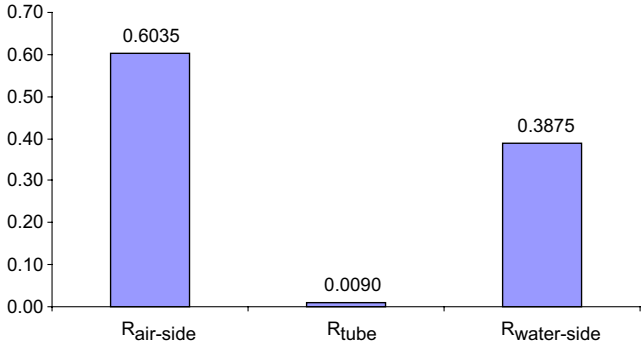

Fig. 12. Distribution of major thermal resistances predicted using the present thermal engineering model for the alternate design carbon-foam finned radiator for thermal conditions corresponding to Test 1 (std).

7. Conclusions

Given the recent interest in the use of porous carbon foam for the construction of finned-tubes, a study has been undertaken to investigate the influence of the foam structure and the fin height, thickness and density on the hydrodynamic and thermal performance of air–water heat exchanger. Engineering models were developed to calculate the hydrodynamic and thermal resistances so that a parametric study could be conducted. The influence of the carbon-foam structure in the engineering models was based on a unit-cube geometry model that describes the internal structure of the foam, the exposed area, the permeability and the effective conductivity as a function of the porosity and pore diameter. Comparisons with measured results obtained from a carbon-foam, finned-tube, air–water radiator showed that the engineering models estimate airside pressure drop and thermal performance within 13.5% and 8.6%, respectively. A parametric study done using the engineering models showed the porosity and fin density have the largest influence on the hydrodynamic and thermal performance of the heat exchanger. An optimization done using the engineering models showed that improvements in thermal performance of up to 15% over conventional aluminum radiators is possible using carbon-foam finned tubes in the simple configuration considered.

Acknowledgements

The authors are grateful to Rob Brandon, David Stinton and Nidia Gallego for many helpful technical discussions. We are also pleased to thank CANMET Energy Technology Centre of Canada's Department of Natural Resources, Oak Ridge National Laboratory, and the US Department of Energy—Office of Distributed Energy for financial support.

References

[1] R.D. Ott, A. Zaltash, W.J. Klett, Utilization of a graphite foam radiator on a natural gas engine-driven heat pump, Proceedings of IMECE'02, 2002 ASME International Mechanical Engineering Conference and Exposition, Louisiana, 2002.
[2] C.N. Gallego, W.J. Klett, Carbon foams for thermal management, Carbon 41 (2003) 1461–1466.

[3] W.J. Klett, R. Hardy, E. Romine, C. Walls, T. Burchell, High-thermal-conductivity, mesophase-pitch-derived carbon foam: effect of precursor on structure and properties, Carbon 38 (2000) 953–973.
[4] Q. Yu, Thermal engineering model for air–water heat exchangers made of carbon foam finned tubes, M.E.Sc. Thesis, The University of Western Ontario, London, Canada, 2004.
[5] C.J. Ward, Turbulent flow in porous media, J. Hydraul. Div., Proceeding of the American Society of the Civil Engineers, ASCE, HY5, 1964, pp. 1–11.
[6] J.R. Tsal, F.H. Behls, R. Mangel, T-method duct design, part III: simulation, ASHRAE Trans. 96 (2) (1990) 3–31.
[7] A.V. Kuznetsov, Analytical studies of forced convection in partly porous configurations, in: K. Vafai, H.A. Hadim (Eds.), Handbook of Porous Media, Marcel Dekker Inc., New York, 2000, pp. 272–273.
[8] N.E. Sieder, G.E. Tate, Heat transfer and pressure drop of liquids in tubes, Ind. Eng. Chem. 28 (1936) 1429–1435.
[9] V. Gnielinski, New equations for heat and mass transfer in turbulent pipe and channel flow, Int. J. Chem. Eng. 16 (1976) 359–367.
[10] R.K. Shah, D.P. Sekulic, Fundamentals of Heat Exchanger Design, John Wiley & Sons, New York, 2003, pp. 114–140.
[11] S.W. Churchill, M. Bernstein, A correlating equation fro forced convection from gases and liquids to a circular cylinder in crossflow, Trans. ASME 99 (1977) 300–306.
[12] M.M. Yovanovich, S.Y. Muzychka, R.J. Culham, Spreading resistance of isoflux rectangles and strips on compound flux channels, J. Thermophys. Heat Transfer 13 (1999) 495–500.
[13] P. Teertstra, M.M. Yovannovich, R.J. Culham, Analytical forced convection modeling of plate fin heat sinks, J. Electron. Manufact. 10 (2000) 253–261.
[14] H.S.R. Winterton, Technical notes: where did the Dittus and Boelter equation come from, Int. J. Heat Mass Transfer 41 (1997) 8809–8810.
[15] F.A.L. Dullien, Porous Media Fluid Transfer and Pore Structure, Academic Press, New York, 1979.
[16] K.K. Kar, A. Dybbs, Internal heat transfer coefficients of porous metals, in: J.V. Beck, L.S. Yao (Eds.), Heat Transfer in Porous Media, ASME, New York, 1982, HTD-22.
[17] G. Lauriat, R. Ghafir, Forced convective heat transfer in porous materials, in: K. Vafai, H.A. Hadim (Eds.), Handbook of Porous Media, Marcel Dekker, New York, 2000, pp. 201–267.
[18] B.W. Gamson, G. Thodos, O.A. Hougen, Heat, mass and momentum transfer in the flow gases through granular solid, Trans. AIChE 39 (1943) 1–35.
[19] G.J. Hwang, C.C. Wu, C.H. Chao, Investigation of non-Darcy forced convection in an asymmetrically heated sinlerted porous channel, ASME J. Heat Transfer 117 (1995) 725–731.
[20] A.S. Headyat, N.J.A. Sloane, J. Stufken, Orthogonal Arrays: Theory and Applications, Springer-Verlag, New York, 1999.